Available online at www.sciencedirect.com
ScienceDirect
Journal of Catalysis 245 (2007) 156–172
JOURNAL OF CATALYSIS
www.elsevier.com/locate/jcat

New supported vanadia catalysts for oxidation reactions prepared by sputter deposition

H. Poelman [a,*], B.F. Sels [b], M. Olea [c], K. Eufinger [a], J.S. Paul [b], B. Moens [b], I. Sack [c], V. Balcaen [c], F. Bertinchamps [d], E.M. Gaigneaux [d], P.A. Jacobs [b], G.B. Marin [c], D. Poelman [a], R. De Gryse [a]

[a] *Surface Physics and Thin Films Division, Department of Solid State Sciences, Ghent University, Krijgslaan 281-S1, B-9000 Ghent, Belgium*
[b] *Centrum voor Oppervlaktechemie en Katalyse, Department of Interphase Chemistry, K.U. Leuven, Kasteelpark Arenberg 23, B-3001 Heverlee, Belgium*
[c] *Laboratorium voor Petrochemische Techniek, Department of Chemical Engineering, Ghent University, Krijgslaan 281-S5, B-9000 Ghent, Belgium*
[d] *Unité de Catalyse et Chimie des Matériaux Divisés, Université Catholique de Louvain, Croix du Sud 2/17, B-1348 Louvain-la-Neuve, Belgium*

Received 13 July 2006; revised 14 September 2006; accepted 25 September 2006

Available online 1 November 2006

Abstract

Model vanadia catalysts were synthesised using magnetron sputtering of the active species for precisely controlled and clean catalyst design. Two series of supported vanadia catalysts were produced on inert beads with silica surface: vanadia/silica through single vanadia coating and vanadia/titania/silica by subsequent deposition of titania and vanadia. Loadings were varied by changing deposition time. All catalysts were characterised for structure and reducibility. Catalytic performance was tested by steady-state and transient experiments with propane oxidative dehydrogenation. Both supports yielded similar vanadia structures and equal dispersion. The vanadia loading strongly influenced structure and chemical behaviour. Shorter depositions gave surface vanadia monomers and polymers, whereas for longer depositions, crystalline species developed on either support. In propane oxidative dehydrogenation, very high turnover frequencies were obtained, especially for thinner depositions. An intermediate titania layer strongly influenced the vanadia activity. Maximum activity was obtained for a few vanadia layers supported on titania.

Keywords: Supported vanadia catalysts; DC magnetron sputtering; Oxidative dehydrogenation; Propane; DRS; TPR; TAP; Transient experiments; Steady-state experiments

1. Introduction

Among the metal oxide catalysts, vanadia-based catalysts have attracted wide interest due to their value in several chemical reactions. Important processes are oxidation reactions [1,2], ammoxidation [3], selective reduction of NO_x [4] and oxidative dehydrogenation [5]. When the vanadia is deposited on an oxide support, a close contact is achieved between the vanadia layer and the support surface. The properties of the latter influence both dispersion and structure of the vanadia species, resulting in chemical reactivity differences compared with unsupported vanadia [6]. In this respect, vanadia supported on titania has drawn much attention because of its enhanced catalytic activity [7].

Despite their importance, several fundamental questions regarding the reactivity of the supported vanadia in relation with the structural appearance remain unsolved. This lack of understanding underlines the need for a supported vanadia model catalyst, synthesised in a fully controllable and clean way. Such a structure would ideally allow performance of a correct basic characterization through both physical and chemical analysis, providing insight into the effect of the titania support decoupled from any preparation or contamination influence.

Traditionally, heterogeneous supported oxide catalysts are prepared by impregnation or coprecipitation of suitable precursors onto an inert carrier [8]. Activation of the desired compounds is usually obtained by calcination, that is, heating in air. Another chemical method is chemical vapour deposition

* Corresponding author. Fax: +32 9 264 49 96.
E-mail address: hilde.poelman@UGent.be (H. Poelman).

0021-9517/$ – see front matter
doi:10.1016/j.jcat.2006.09.022

(CVD), in which a suitable precursor is transported through the gas phase and adsorbed on the support's surface. The catalyst layer is then formed through chemical reaction [9–11]. These chemical techniques exhibit some intrinsic drawbacks. One of them is that foreign material (from, e.g., solvent or precursor) can be included in the deposition, resulting in contamination. Moreover, the V species that result from the preparation depend not only on the support (e.g., its surface charge, cleanliness, presence of adsorbents) but also on the solution or gas-phase properties.

Applying physical techniques instead offers a new approach to the synthesis of heterogeneous catalysts. In these physical methods, the desired element or compound is brought into the gas phase, from where it travels to the substrate. This gas-phase state can be achieved through thermal or electron beam evaporation, or through sputter deposition. If a compound is required, (e.g., an oxide or nitride), one can start from either the elemental source material or a compound source. In the former case, a stoichiometric compound is obtained by either reactively depositing the source material (i.e., the vaporized or sputtered elements can react with a reactive gas to form a compound) or by performing a postdeposition annealing. Physical vapour deposition (PVD) techniques are advantageous in that they provide very high controllability and reproducibility, are applicable to a wide variety of catalyst materials (some of which even cannot be prepared classically), and ensure clean sample preparation [12].

Among the physical deposition techniques, DC magnetron sputtering is well established for the production of thin films. It is highly controllable and provides good adhesion as well as good coating uniformity, due to the relatively high energy of the deposited particles. The growth process has been described following several models, depending on substrate and layer material and adatom mobility [13]. In general, sputter deposition supplies additional energy to the deposited material. The discharge causes unintentional heating of the substrate (typically 350 K) and negative plasma ions, secondary electrons, and energetic neutrals can bombard the substrate and the deposited film. This additional energy results in sputter cleaning of the substrate and densification of the deposited film because adatoms acquire sufficient energy to diffuse to energetically more favourable sites, thus filling pits and voids. As a result, homogeneous coverage of the substrate occurs, irrespective of the support.

Although sputter deposition is widespread for the production of thin films on flat surfaces, to date it has scarcely been used for the coating of small particles. To achieve a homogeneous coating of such supports, one needs to expose all sides to the flux of sputtered material. Because in first approximation, sputter deposition is a line-of-sight process, this can be achieved by continuous motion of the particles, either through mechanical vibration or by a rotating vessel. Few publications report on the sputter deposition of metal films such as Au, Pt, or Cu on powder supports [14–16].

To the best of our knowledge, to date no mention has been made of sputter-deposited oxides onto small particles for catalytic purposes. The sputter deposition of oxide layers is, however, widely used in thin film applications, such as interference filters, antireflective coatings, and photocatalytically active coatings for air and water cleaning. It requires the addition of oxygen as a reactive gas to the sputter plasma or a postdeposition annealing to obtain fully oxidised layers.

In an attempt to obtain fundamental insight into the effects of the structure and support not hindered by contamination or preparation effects, supported vanadia catalysts were synthesised by means of reactive DC magnetron sputtering onto small inert particles in a rotating drum as a novel method. Apart from the layer–support interaction, the properties of these sputter-deposited catalysts are determined only by the specific sputter conditions of their deposition, which are highly reproducible. Hence, they can be referred to as model catalysts. The objective of the present work is then to determine the basic characteristics of these catalysts by physical and chemical means and to examine the origin of the titania support effect. Therefore, comparison is made between sputter-deposited vanadia/titania and vanadia/silica catalysts, the latter being reported to yield worse dispersion [5,6]. The catalyst properties are compared with appropriate literature results on supported vanadia catalysts.

2. Catalyst synthesis

Supported vanadia (VO_x) catalysts were synthesized by means of DC magnetron sputter deposition of the active layers in an argon/oxygen atmosphere onto spherical inert beads, SiO_2–ZrO_2 (33 wt% SiO_2, 67 wt% ZrO_2, 250–425 μm diameter, ZIR337, Phibo Industries) [17]. The beads were introduced into a rotating drum, with a load capacity up to the kilogram scale, within a vacuum system (base pressure $<10^{-3}$ Pa). Vanadia was deposited either directly onto the inert beads or onto beads that were first coated with titania [18]. In this way, two different supports for the vanadia were obtained, allowing an evaluation of their influence.

The titania coating was applied using a rotatable cylindrical magnetron (14 cm diameter, 45 cm long) with a plasma-sprayed TiO_2 rutile target (Bekaert Advanced Coatings, Deinze, Belgium). When operated in reactive sputter mode (i.e., by adding oxygen as reactive gas component to the sputter gas), this kind of target has proven to yield depositions of near-stoichiometric TiO_2 in the anatase phase.

For the vanadia sputter deposition, two plane circular magnetrons (5 cm diameter) were mounted side by side in the centre of the rotating drum, facing downward. They were charged with ceramic V_2O_3 targets (supplied by ITME, Warsaw, Poland), yielding near-stoichiometric V_2O_5 depositions when operated with suitable sputter conditions in reactive sputter mode [19].

All targets were presputtered for at least 10 min to assure stable operation. Deposition times were 180 min for titania (sample label Ti) (pressure, 0.71 Pa; power, 2500 W; O_2/Ar flow ratio, 1.5/7.1) and 5, 15, 30, 60, 150, and 330 min for vanadia (labeled V*time*; *time* = vanadia deposition time in minutes) (pressure, 1.8 Pa; power, 2 × 100 W; O_2/Ar flow ratio, 1.5/6). All titania layers received postdeposition annealing at 623 K for 1 h in air to favour full oxidation toward TiO_2 (label subscript H). After the final vanadia deposition, each catalyst batch received a final annealing (623 K, 1 h, air) to improve stoichiometry. The

latter resembles the traditional temperature treatment in classical catalyst preparation, in which it acts as activation step. Moreover, it helps homogenize the sputter-deposited coating, because vanadia easily diffuses at relatively low temperatures. Indeed, V_2O_5 exhibits a low T_{tamman} (482 K [20,21]), the temperature at which diffusion becomes significant. Samples were labelled following the consecutive steps in their synthesis; for example, Ti_HV60_H was first coated with titania for 180 min, annealed, then coated with vanadia for 60 min, and again annealed.

3. Experimental

3.1. Physical characterization

Crystallinity of the depositions was checked by means of X-ray diffraction measurements in θ–2θ mode (XRD; Bruker-AXS D8 Discover with linear position sensitive detection segment, covering 12°; measuring time, 1076 s step^{-1}). Atomic force microscopy in contact mode (AFM; Topometrix TMX 2010; force constant 0.01 N m^{-1}), as well as scanning electron microscopy (SEM; FEI Quanta 200F), were performed to evaluate the surface morphology of the beads and depositions. An acceleration voltage of 25 or 12.5 kV was chosen for the secondary electron SEM images.

To visualise the deposited layers, transmission electron microscopy (TEM) was performed on the sample with the longest vanadia deposition on a titania-coated bead, Ti_HV330_H. The sample thickness was reduced by mechanical polishing and focussed ion-beam milling. Bright-field and high-resolution TEM, as well as chemical mapping by energy-filtered TEM (EFTEM), were applied. A JEOL 3000F FEG electron microscope, operated at 300 kV and with a point resolution of about 2 Å, was used.

The specific surface area of the samples was measured by the BET method using a Micromeretics ASAP 2000 instrument by krypton adsorption at 77 K on 1 g of sample. Before the measurements, all samples were outgassed at 423 K in vacuum (1.33×10^{-3} Pa).

EDX (EDAX inc.) at 17.5 kV acceleration voltage provided a first analysis of the bare support, typically in a 1-μm-thick volume. A full elemental composition of the coated beads was obtained by ICP-MS analysis (IRIS Advantage system, Thermo Jarrell Ash) by acid dissolution in HNO_3, HF, and $HClO_4$. All catalysts were dried at 338 K before dissolution.

Surface composition was determined by means of XPS measurements with a Perkin-Elmer PHI ESCA 5500 system equipped with a monochromatic 450-W Al$K\alpha$ source (base pressure $<10^{-7}$ Pa). Numerous beads were spread onto carbon tape, and a detection mode was chosen so as to cover several beads. Wide-scan surveys and high-resolution multiplex measurements were performed on all samples (pass energy, 187.85 and 58.70 eV, respectively).

To learn about the vanadium coordination on the sputter-deposited catalysts, Raman measurements were attempted using a Labram spectrometer (Dilor) interfaced with an Olympus optical microscope. The excitation radiation was a He–Ne laser (632.8 nm, 10 mW). The 10×, 50×, and 100× objectives of the microscope were used, so that spots of about 50, 10, and 5 μm^2 at the surface of the sample were measured. Spectra were obtained by averaging 10 scans of the Raman shift range between 200 and 1200 cm^{-1} recorded over 120 s with a spectral resolution of 7 cm^{-1}.

In addition, the local structure and degree of polymerization was studied using diffuse reflectance spectroscopy (DRS UV–vis). This technique was performed with a Varian Cary 5 spectrophotometer equipped with an integrating sphere accessory at 200–800 nm, referenced to $BaSO_4$. The samples were dried in a dry air flow at 773 K before measurement. The absorption spectra were recorded in the diffuse reflectance mode (R) and transformed to a magnitude proportional to the extinction coefficient (K) through the Kubelka–Munk function [$F(R_\infty)$].

3.2. Catalytic performance

3.2.1. H_2 reducibility (TPR)

Hydrogen temperature-programmed reduction (TPR) was performed to determine the reducibility of the catalysts and thereby their reactivity. TPR profiles were obtained in a home-made facility using MS detection (Pfeiffer Omnistar quadrupole mass spectrometer) under the following conditions: sample weight 5 g, heating rate 10 K min^{-1}, flow rate 10 ml min^{-1}, and 5% H_2 in N_2. Before the reduction measurements, the samples were calcined in air at 773 K for 3 h and cooled to 373 K under He flow (20 ml min^{-1}).

3.2.2. Continuous-flow steady-state experiments

The catalytic performance of the sputter-deposited catalysts was tested by means of oxidative dehydrogenation (ODH) of propane as model reaction. Oxidation reactions were performed in a custom-made fixed-bed continuous-flow reactor equipped with four parallel microreactors. Each catalyst (1.0 g) was pretreated at 773 K in 20 vol% O_2 in helium (30 ml min^{-1}). It was then cooled under O_2/He flow to 723 K. For the reaction, a feed of 20 vol% propane (20 ml min^{-1}) and 10 vol% O_2 balanced with helium was applied. The temperature was increased under reaction conditions in steps of 25 K up to 823 K at a rate of 5 K min^{-1} and kept constant for 400 min at each temperature. During this time-on-stream, several samples were obtained under steady-state conditions. Feed and products were analyzed with an on-line HP 5890 Series II gas chromatograph equipped with a Poraplot Q column connected to a flame ionization detector with an internal methanizer in the jet. Under these conditions, the carbon balance was generally >96%. A control measurement at 723 K at the end of the temperature cycle showed that no deactivation of the catalyst occurred during the steady-state experiments.

3.2.3. Temporal analysis of products experiments

The gas–solid interactions over the sputter-deposited catalysts were also investigated by transient measurements using the temporal analysis of products (TAP) technique, which allows state-by-state screening [22]. A detailed description of the

TAP reactor system has been given previously [23]. Single-pulse, multi-pulse, and alternating-pulse experiments for ODH of propane were performed.

The catalyst bed ($\leqslant$1 g) was packed in the reactor between two layers of quartz of the same particle size (250–425 μm). Each sample was heated to the reaction temperature of 773 K at a heating rate of 5 K min^{-1} and then pretreated at this temperature by pulsing 3×10^{18} oxygen molecules to reach a completely oxidized state.

In both the single-pulse and alternating-pulse experiments, 10 pulses were repeated and the responses averaged to improve the signal-to-noise ratio. The number of molecules admitted per pulse was in the range of 10^{14}–10^{15}, allowing transport in the reactor to occur through Knudsen diffusion only. In one pulse, the ratio of admitted propane to the vanadium loaded in the reactor was always <0.04, to avoid changing the catalyst's state. Multipulse experiments were performed to study the interaction of the model molecule with the surface at a certain degree of reduction. A reduced state was reached by pulsing 7.5×10^{18} molecules of propane over a completely oxidized surface.

4. Physical characterization results

4.1. Supports

4.1.1. Bare beads

The bare SiO_2–ZrO_2 beads resembled white spheres and consisted of crystalline zirconia granulates embedded in an amorphous silica matrix, as determined from XRD, EDX (both not shown), and SEM (Fig. 1). The outer surface consisted of silica binding material, which is where the sputter deposition occurred. An AFM measurement on a single bare bead was performed to assess the surface roughness (not shown). The surface was smooth, and the surface area for a 5 × 5 μm image, calculated by taking into account the measured profile, was hardly larger than the geometrical one (25.58 vs 25 μm^2).

BET measurements showed that the specific surface area was below the BET detection limit (typically 0.1 m^2 g^{-1}). Hence, the SiO_2–ZrO_2 support is a truly nonporous solid. From particle size distribution measurements, the average geometric surface area for the range of bead diameters used was determined to be 0.0049 m^2 g^{-1} (±0.0002 m^2 g^{-1}).

Table 1
Elemental and surface composition of bare beads as obtained from ICP and surface XPS analysis, respectively; XPS values balanced with O

	Si	Zr	Al	Ti	V
ICP (mol kg^{-1})	4.5	4.8	0.9	0.015	0.0014
Surface XPS (at%)	21.75	2.6	6.9	–	–

A full elemental composition was obtained from ICP analysis of the bare beads (Table 1). Some Al was found together with traces of Ti and V. Their presence in the SiO_2–ZrO_2 support originates from the manufacturing process of the beads. A surface XPS analysis confirmed that the surface contains mostly Si, along with Al and Zr (Table 1).

4.1.2. Titania-coated beads

An XRD spectrum of titania-coated beads showed a weak diffraction line from TiO_2 among the zirconia lines (Fig. 2). Inspection of its position ($2\theta = \sim 25.5°$) indicated that this line corresponded to either anatase (101) or brookite (120), definitely not to rutile. Because titania sputter deposition plus subsequent annealing has proven to yield anatase layers [24], we can conclude that the sputter-deposited titania is most probably polycrystalline anatase.

The titania deposition could be distinguished faintly with SEM (not shown). From AFM, the surface appeared roughened compared with the uncoated beads (not shown), and the effective surface area for Ti_H was now 26.3 μm^2, about 5% larger than for the bare beads.

ICP analysis of the titania-coated beads Ti_H yielded 0.0042 mol Ti kg^{-1} in addition to the Ti already present as trace contamination inside the beads. Taking into account the TiO_2 density as well as the density and average dimensions of the beads (see Section 4.1.1), this corresponds to a 19.5-nm (±3.4 nm)-thick titania coating. XPS showed that the surface consisted mainly of titania, with only ca. 2 at% Si detectable. Note that for the kinetic energy of Ti2p photoelectrons in the XPS system used, the XPS information depth amounted to several atomic layers. The Ti2p signal consisted of a main Ti^{4+} contribution, with a Ti^{3+} component (±20%); thus, the deposited titania was substoichiometric TiO_x.

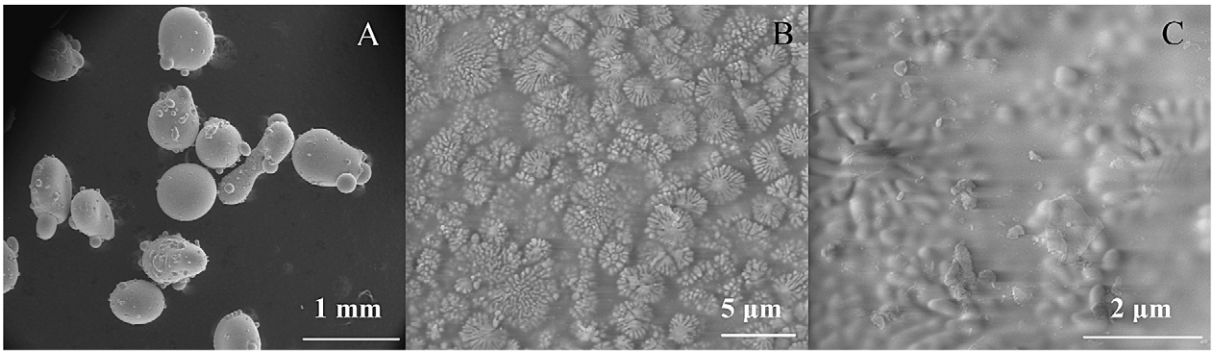

Fig. 1. Secondary electron images (SEM) of the bare beads: (A) collection of beads, (B) detail of bead surface showing a number of 'granulates,' (C) detail of 'granulates.'

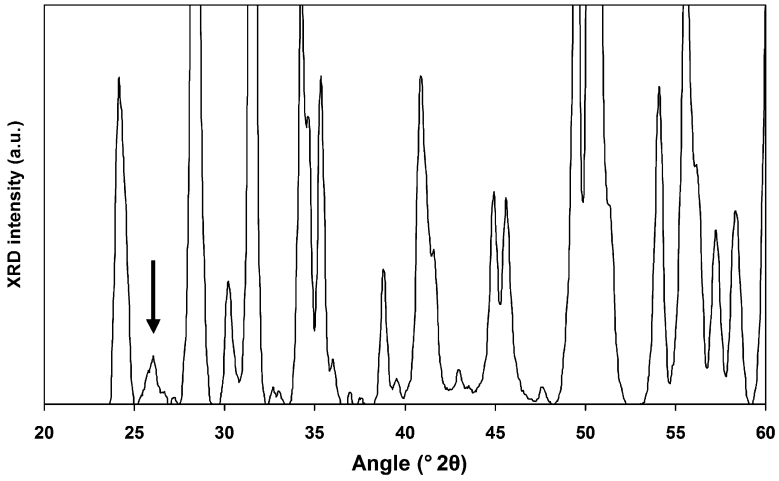

Fig. 2. XRD of titania coated beads (sample Ti_H) in θ–2θ mode; all major lines originate from zirconia; marked peak: anatase (101) line.

Table 2
V loading from ICP, calculated thickness, apparent surface density and theoretical number of polyvanadate layers for vanadia/silica (left part) and vanadia/titania catalysts (right part)[a]

	Sample											
	$V5_H$	$V15_H$	$V30_H$	$V60_H$	$V150_H$	$V330_H$	Ti_HV5_H	Ti_HV15_H	Ti_HV30_H	Ti_HV60_H	Ti_HV150_H	Ti_HV330_H
V loading (10^{-4} mol kg^{-1})	<0.1	0.17	0.66	3	8	13	0.48	0.69	2	3	7	11
VO_x thickness (nm)	0.0 (±0.1)	0.1 (±0.3)	0.4 (±0.2)	1.6 (±0.2)	4.3 (±0.5)	7.0 (±0.6)	0.2 (±0.1)	0.4 (±0.1)	0.8 (±0.2)	1.4 (±0.4)	3.7 (±0.7)	5.5 (±0.5)
Apparent surface density (V nm^{-2})	<2.0 (±2.4)	2.0 (±2.6)	8.1 (±3.1)	36.5 (±3.3)	96.5 (±5.4)	157.6 (±7.9)	5.6 (±2.4)	8.0 (±2.4)	18.2 (±2.5)	31.0 (±2.6)	83.9 (±4.6)	123.9 (±6.3)
Polyvanadate layers	<0.8 (±1.0)	0.8 (±1.1)	1.7 (±0.7)	5.5 (±0.7)	13.5 (±1.2)	21.7 (±1.8)	0.7 (±0.3)	1.1 (±0.3)	2.4 (±0.4)	4.1 (±0.5)	11.2 (±1.0)	16.5 (±1.4)

[a] Error ranges in parentheses are based on standard error calculations.

4.2. Supported vanadia catalysts

4.2.1. Silica-supported vanadia

A series of silica-supported vanadia catalysts with variable loadings was obtained by varying the deposition time. After the postdeposition annealing, vanadia/silica labels run as V*time*$_H$. The shortest depositions were not visible to the naked eye, but after 60 min deposition time, a yellowish aspect developed, reflecting the characteristic yellow-brown colour of V_2O_5. An XRD spectrum taken from the catalyst with longest deposition time, $V330_H$, showed the deposition to be XRD-amorphous (i.e., too thin to yield diffraction lines) or truly amorphous, thus without long-range order (not shown).

SEM showed the vanadia deposition of sample $V330_H$ as a cloud-like coating (not shown), and an AFM image (not shown) yielded an effective surface area of 26.4 μm^2. The absolute amount of deposited V, determined by ICP, increased with deposition time up to 0.0013 mol kg^{-1} for $V330_H$ after correction for the intrinsic V contamination of the beads. From these values, taking into account the V_2O_5 density as well as the density and specific surface area of the beads (see Section 4.1.1), a vanadia thickness was calculated. Table 2 lists both V loading and calculated thickness for all six vanadia deposition times with the estimated error range. Given the thickness of a bulk-like V_2O_5 sheet or lamella of 0.44 nm [25], a V_2O_5-like "monolayer equivalent" was present for a vanadia sputter time of about 30 min.

XPS measurements showed an increasing amount of V at the surface as a function of deposition time, covering Si and Zr from the bare beads. For the longest deposition time, 330 min, the Zr signal almost disappeared, and Si decreased considerably. The V/Si ratio varied from 0.02 for $V5_H$ up to 2.55 for $V330_H$. Just as for Ti2p, the V2p kinetic energy was such that XPS information depth amounted to several atomic layers.

From ICP and XPS, the dispersion of the vanadia deposited onto the silica surface was evaluated by plotting the ratio V/all = V/(V + Si + Zr + Al) at the surface versus the net V loading (Fig. 3). The resulting graph showed a linear relationship, indicating that the increasing amount of deposited vanadia remained well spread over the (silica) surface of the beads. Hence, sputter deposition provides an adequate synthesis method for applying well-dispersed vanadia layers onto a silica support.

Fig. 4 presents the UV–vis diffuse reflectance spectra of the vanadia/silica catalysts V*time*$_H$ after subtraction of the contribution of the SiO_2–ZrO_2 support. The latter is shown in the inset as a reference, displaying absorption bands with maxima at about 42,700 cm^{-1} and near 34,000 cm^{-1}, indicative of crystalline ZrO_2 [26]. Amorphous silica does not give rise to absorption bands in the measured range [27].

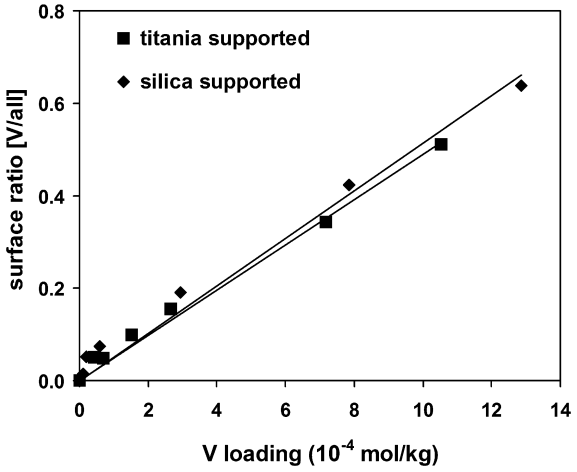

Fig. 3. Variation of the surface ratio V/all (from XPS) versus the net V loading in the layers (from ICP), where 'all' indicates (V + Si + Zr + Al) for vanadia/silica, resp. (V + Ti + Si) for vanadia/titania.

Analysis of the intense ligand-to-metal $O^{2-} \rightarrow V^{5+}$ charge transfer (LMCT) bands and the weaker d–d transitions in DRS spectra provides information concerning the oxidation state and coordination of the central V cation. In the case of supported vanadia, energy absorption in the region of 20,000–30,000 cm^{-1} is due to polymerized octahedrally coordinated V^{5+} [28–30], whereas bands in the region of 30,000–35,000 cm^{-1} are typical for V^{5+} in tetrahedral coordination [31–33]. Absorption bands situated at wave numbers above 35,000 cm^{-1} are characteristic of isolated tetrahedrally coordinated V^{5+} or for d–d transitions in V^{4+}.

Because all catalysts were calcined before DRS measurements, the V^{4+} species present will be oxidised, and hence no V^{4+} contributions are expected to occur. From Fig. 4, catalysts with shorter deposition times $V5_H$ and $V15_H$ show only a weak contribution in the range of tetrahedrally coordinated V^{5+}. $V60_H$ already exhibits stronger bands, shifting toward a more intermediate position between tetrahedral and octahedral contributions, whereas in $V150_H$ and $V330_H$ the latter are dominant.

4.2.2. *Vanadia supported on titania-coated beads*

By varying the vanadia deposition time on titania-coated beads, a series with variable V loadings was obtained and after postdeposition annealing, vanadia/titania labels run as $Ti_HV\mathit{time}_H$. The presence of vanadia is obvious by the colour from 60 min deposition time on (Ti_HV60_H and longer). An XRD spectrum taken from the catalyst with longest deposition time, Ti_HV330_H, again contained a weak diffraction line from TiO_2 among the zirconia lines (not shown). On the other hand, for the vanadia, the depositions remained XRD-amorphous.

SEM on Ti_HV330_H showed the double deposition as a cloudy coating (not shown). The surface area for Ti_HV330_H calculated from AFM was 27.0 μm^2, slightly larger than for the original beads. On the same sample, TEM was undertaken to visualise the depositions. Fig. 5 shows a TEM image of a selected area (Fig. 5A), as well as the EFTEM chemical maps for the elements Ti, V, Si, and Zr (Figs. 5B–5E). Both layers can be observed. The thickness of the titania layer varied between 15 and 30 nm, as seen from its chemical map (see Fig. 5B), whereas that of the vanadia layer was estimated as 7–30 nm (see Fig. 5C). Under high-resolution conditions, the deposited layers exhibit lattice contrast at high magnification, indicating the presence of at least one nanophase for each deposited oxide, with some degree of crystalline ordering (not shown).

The net amount of deposited Ti (0.0044 mol Ti per kg of catalyst) was similar to the Ti content of the singly coated beads Ti_H, and corresponds to an estimated thickness of 18.4 nm (±3.4 nm). The net amount of V increased from

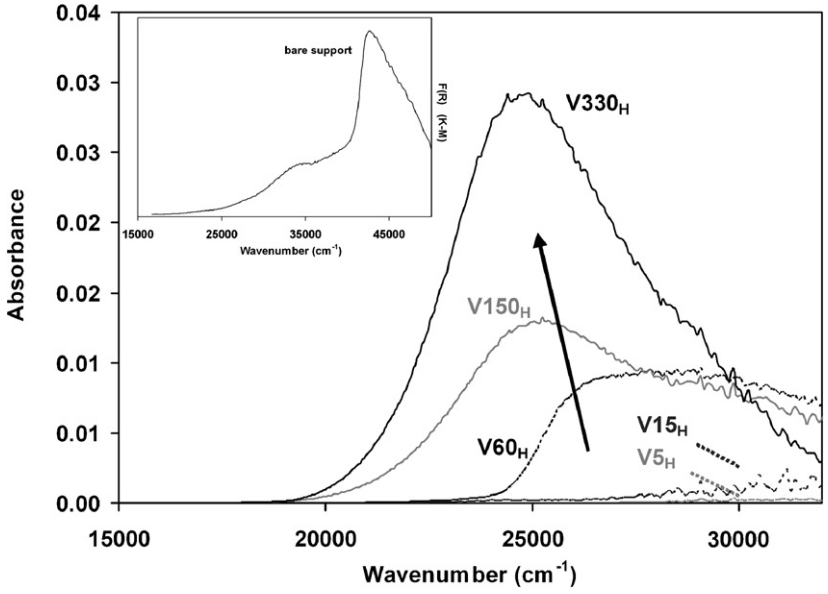

Fig. 4. DRS spectra of vanadia/silica catalysts, $V\mathit{time}_H$ (time = 5, 15, 60, 150, and 330 min vanadia deposition time), obtained via sputter deposition of vanadia directly on the SiO_2–ZrO_2 support material. The contribution of the bare beads SiO_2–ZrO_2 has been subtracted. The arrow indicates the evolution of the band for octahedral vanadia with increasing deposition time. Inset: DRS spectrum of the SiO_2–ZrO_2 support.

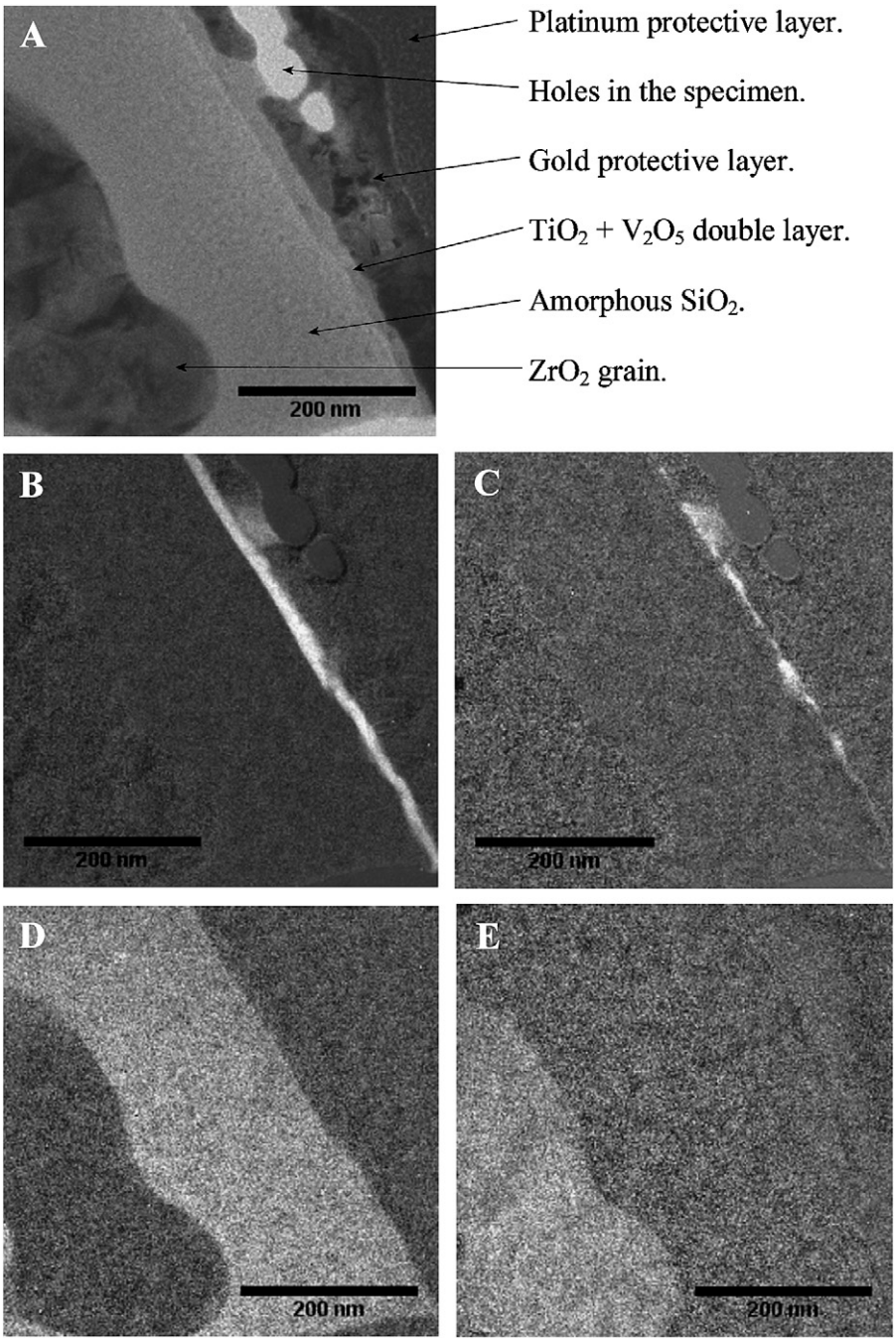

Fig. 5. TEM picture of a selected area on sample Ti_HV330_H (A) and EFTEM chemical mappings of the same area: (B) Ti, (C) V, (D) Si, (E) Zr. A white colour indicates high concentration of the mapped element.

4.8×10^{-5} mol kg^{-1} for Ti_HV5_H up to 1.1×10^{-3} mol kg^{-1} for Ti_HV330_H. Following these values, the vanadia thickness on the vanadia/titania catalysts was calculated. However, because the SEM and AFM images for Ti_H indicated a somewhat roughened surface compared with a bare bead's surface, a 5% larger specific surface area was used. This corresponds to the increase in surface area as evaluated from the AFM image (see Section 4.1.2). Table 2 reports both V loading and thickness with estimated error for all deposition times. Here the equivalent thickness of a single V_2O_5-like layer is obtained for a deposition time of around 15 min, assuming homogeneous coverage.

XPS measurements on the vanadia/titania catalysts revealed an increase of the V surface concentration with deposition time. Because hardly any support signal was detected, it was concluded that the consecutive coating with titania and vanadia covered the bulk support. The V/Ti ratio varied from 0.06 for Ti_HV5_H to 1.62 for Ti_HV330_H.

The dispersion of vanadia was evaluated by plotting the V/all = V/(V + Ti + Si) fraction for the surface, obtained from XPS, versus the net V loading as determined from ICP (Fig. 3). Similar to the silica-supported vanadia, a linear relationship appeared, indicating that the vanadia was homogeneously dispersed over the titania-coated beads.

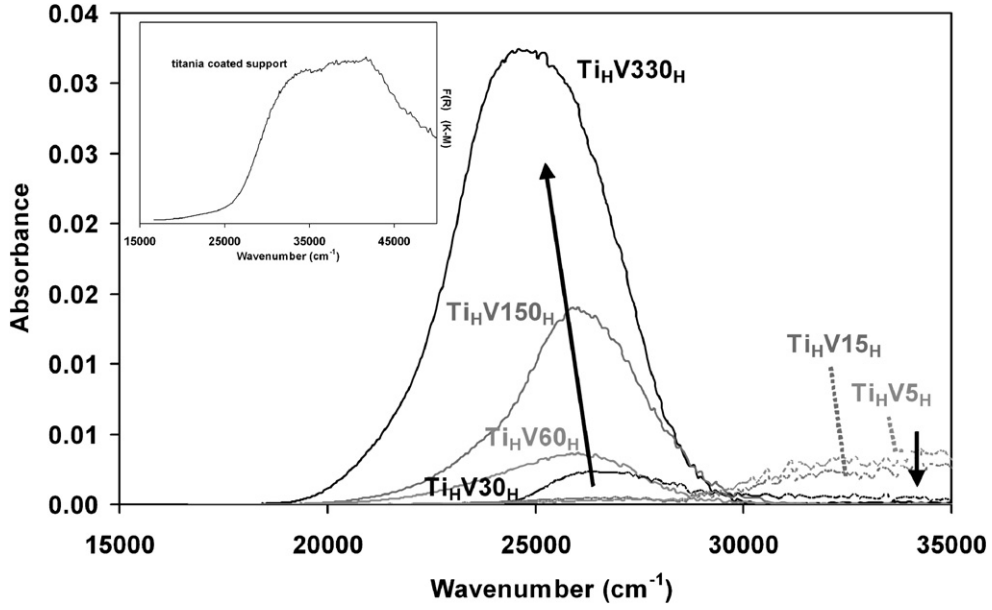

Fig. 6. DRS spectra of vanadia catalysts supported on titania, Ti_HVtime_H (time = 5, 15, 30, 60, 150, and 330 min vanadia deposition time), obtained by vanadia sputter deposition on the titania coated support material. The spectra were corrected for the contribution of titania coated beads by subtraction of the Ti_H spectrum. Arrows indicate the evolution of the major features with increasing deposition time. Inset: DRS spectrum of the titania coated beads, Ti_H.

Although V loadings in the sputter-deposited catalysts were very low, an attempt was made to determine the nature of the deposited vanadia species by means of Raman spectroscopy on Ti_HV330_H, with Ti_H, $V330_H$, and bare beads for comparison. The time of scanning was chosen to saturate the detector with the bands of the bare beads to improve the detection of the bands of titania and vanadia phases. Unfortunately, independent of the microscope objective used, the spectra of all coated samples were similar to the spectrum of the bare beads. Hence, Raman is not sensitive enough to detect the vanadia species in the sputter-deposited catalysts.

Fig. 6 reports the DRS spectra of the vanadia/titania catalysts Ti_HVtime_H after subtraction of the Ti_H support contribution. The latter is shown in the inset as a reference, displaying the titania band in the region between 40,000 and 25,000 cm^{-1} due to $O^{2-} \rightarrow Ti^{4-}$ ligand-to-metal charge transfer (LMCT). The edge energy of this absorbance was situated near 27,000 cm^{-1}, in the region typical for anatase [27]. Because the edge energy of rutile is near 24,000 cm^{-1}, it can be concluded that the deposited TiO_x was mainly in the anatase phase. In the main DRS spectra, two broad absorbance regions appeared: at 45,000–30,000 cm^{-1} due to tetrahedrally coordinated V^{5+} [31–33] (cut to 35,000 cm^{-1} in Fig. 6) and at 30,000–20,000 cm^{-1} due to octahedrally coordinated V^{5+} [28–30], respectively. With increasing V loading, the low energy absorbance increased at the expense of the higher energy absorbance.

5. Catalytic performance results

5.1. Reducibility (TPR)

The reduction behaviour of the surface active vanadium species on doubly coated catalysts, Ti_HVtime_H, was examined by TPR using hydrogen (Fig. 7) [34]. Measurements

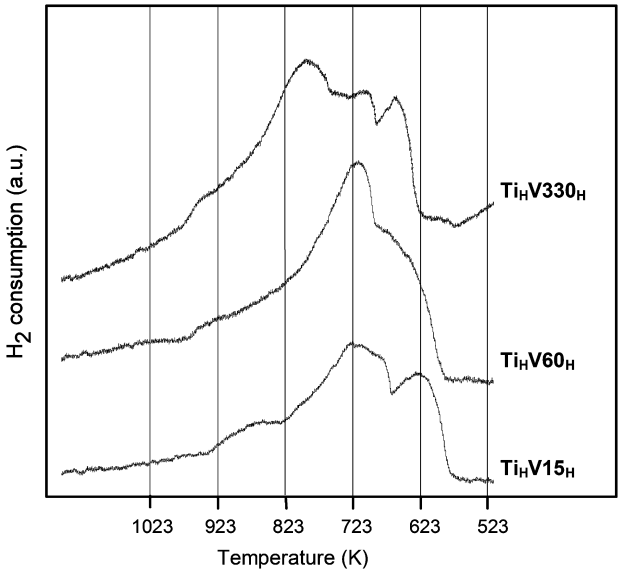

Fig. 7. TPR profiles of Ti_HVtime_H samples Ti_HV15_H, Ti_HV60_H, and Ti_HV330_H (heating rate 10 K min^{-1}, flow rate 10 ml min^{-1}, 5% H_2 in N_2).

were performed on a few representative samples: Ti_HV15_H, Ti_HV60_H, and Ti_HV330_H, corresponding to low, medium, and high vanadia loadings. In all profiles, several contributions were present, reflecting the H_2 reducibility of several species. For catalyst Ti_HV15_H, temperature maxima were seen at 620, 720, and 870 K and a shoulder was observed at 680 K. For catalyst Ti_HV60_H, the signal at 870 K completely vanished. The 720 K signal intensified to become the dominant contribution; the 620 K signal weakened, forming a broad shoulder on the low-temperature side of the dominant 720 K peak. Around 950 K, a new contribution appeared as a weak feature. Catalysts with the longest VO_x depositions showed peaks at 660,

705, and 800 K and a still weak, although distinct contribution at 950 K.

Observing the evolution of T_{onset} throughout the profiles shows that T_{onset} shifted toward higher temperatures with increasing deposition time. A similar trend can be distinguished when focusing on the T_{max} of the dominant features in each profile. Hence, general reducibility decreased with increasing vanadia content. Note that, despite the high resolution of the profiles and the reproducible peak position of the T_{max}, extraction of reliable quantitative information such as the V reduction level could not be performed, because of the low amount of V in the reactor.

5.2. Steady-state experiments

After the catalyst characterization, tests were performed to evaluate their catalytic performance. The oxidative dehydrogenation of propane was chosen as model reaction. Experiments were run with both series of sputter-deposited catalysts V*time*$_H$ and Ti_HV*time*$_H$.

Steady-state experiments were performed at 823 K over catalysts Ti_HV*time*$_H$ and four singly coated catalysts, $V15_H$, $V60_H$, $V150_H$, and $V330_H$. Conversions were low over all catalysts, due to the low amount of vanadia present, but well above and distinct from the conversions of the empty reactor, bare beads, and titania-coated beads, Ti_H.

When taking into account the V loading, the turnover frequency (TOF) for propene formation calculated as activity per (outer surface) V atom turned out to be quite high (>0.2 $mol_{propene}$ mol_V^{-1} s^{-1} at 823 K), especially for the shorter vanadia deposition times supported on titania (Fig. 8). In the TOF calculation, only the fraction of V present at the outer surface of the deposition was taken into account, because these were the only vanadium atoms directly accessible for adsorption/reaction.

Catalysts Ti_HV5_H to Ti_HV60_H showed a comparably high activity when taking into account the error bars, with a slightly pronounced maximum activity for Ti_HV60_H. For longer deposition times, the activity dropped significantly. Note that the activity of vanadia/titania catalysts always remained above the corresponding activity for vanadia/silica, indicating that the titania support layer had a positive influence on the ODH activity of supported vanadia. For the longer deposition times of 150 and 330 min, the activities of both catalyst series converged, reflecting the increasing thickness of the vanadia deposits and hence the gradual suppression of the influence of the underlying TiO_x layer.

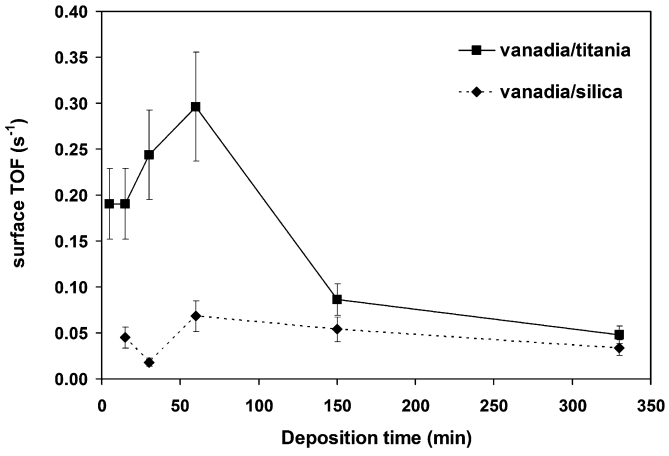

Fig. 8. Turnover frequencies for sputter deposited catalysts Ti_HV*time*$_H$ and singly coated samples $V15_H$, $V30_H$, $V60_H$, $V150_H$, and $V330_H$ (823 K; 20 vol% propane at 20 ml min^{-1}, 10 vol% O_2 balanced with helium); only the outer surface V atoms are taken into account.

5.3. TAP analysis

5.3.1. Activity of the support

Reference information on the activity of the supports was obtained by analysing the TAP results from bare beads—presenting essentially a silica surface (see Section 4.1.1)—and annealed titania-coated beads, Ti_H. Both supports were tested, either completely oxidized or in a partially reduced state, attained after pulsing 7.5×10^{18} propane molecules at 773 K. Single-pulse experiments with propane over the supports yielded quasi-identical response curves, independent of the type of support or its pretreatment (results not shown). The latter observation indicated that propane did not adsorb onto the support surface, so that the shape of the response curve was determined mainly by the Knudsen diffusion coefficient.

Quantitative analysis indicated a conversion of 3% of propane on Ti_H, irrespective of the pretreatment. Propene, CO_2, and water were the main reaction products. The reaction was confirmed by a reoxidation experiment involving a single pulse of oxygen over the same supports. Whereas bare beads again appeared to be inactive, the Ti_H sample did show small differences in oxygen response; Ti_H that was reduced with multiple pulses of propane showed a shift to slightly shorter response time and a narrower response curve compared with a fully oxidized Ti_H sample (Fig. 9). Indeed, an oxygen conversion of 18% was found on reduced Ti_H.

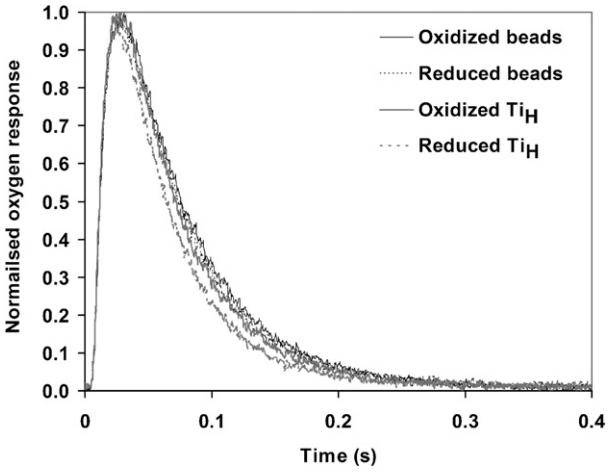

Fig. 9. Normalized response of oxygen as a function of time at 773 K. Single pulse experiment of oxygen over bare beads and titania coated beads, Ti_H, either completely oxidized or after pulsing 7.5×10^{18} propane molecules (reduced). The number of molecules admitted per pulse was in the range of 10^{14}–10^{15} molecules.

5.3.2. Activity of titania-supported vanadia catalysts: influence of deposition time

Compared with the support Ti_H, a higher catalytic activity was obtained for the vanadia/titania catalysts. The variation of propane conversion for Ti_HVtime_H with vanadia deposition time was very similar to the steady-state result, yielding a maximum conversion in propane ODH over Ti_HV60_H (not shown). No distinction could be made between sputter-deposited catalysts with the shortest deposition times of 5, 15, and 30 min. The propane reducibility and consecutive reoxidation of the Ti_HVtime_H catalysts were tested by means of TAP experiments. A predefined number of propane pulses (multiple-pulse experiment: 7.5×10^{18} molecules in total; propane:V atom ratio >20:1; 773 K) was sent over the completely oxidized catalysts, and their new, reduced state was assessed by comparing the propane response from single-pulse experiments, performed before and after the multiple-pulse experiment. The degree of reduction was then defined as the ratio of the number of oxygen atoms removed from the catalyst, leaving free reduced sites, to the total deposited vanadia content [35]. The catalysts with 5, 15, 30, and 60 min deposition time were completely reduced, whereas the degree of reduction was only 0.75 for the Ti_HV150_H and 0.63 for Ti_HV330_H. The reoxidation reaction of these reduced catalysts has been found to follow an irreversible dissociative oxygen chemisorption mechanism [35].

To assess the influence of weakly adsorbed oxygen in the ODH reaction over the sputter-deposited catalysts, an alternating-pulse experiment was performed over the Ti_HV330_H catalyst. Oxygen (pump molecule) was pulsed first over the catalyst, followed by propane (probe molecule) at different time intervals. No reaction products were observed on the oxygen pulse. On the propane pulse, the reaction products followed were CO_2 and propene. Fig. 10 presents the propane conversion and CO_2 and propene yield as a function of time interval. Conversion was found to decrease up to a 0.07 s time interval, which corresponds to the lifetime of weakly adsorbed oxygen [36]. For longer time intervals, the conversion remained almost constant. Because weakly adsorbed oxygen species were by then no longer available, from there on only lattice oxygen took part in the reaction with propane. For time intervals up to 0.07 s, propane reacted with preadsorbed oxygen as well. Because the CO_2 yield decreased with increasing time intervals up to 0.07 s while the propene yield remained constant, we conclude that weakly adsorbed oxygen species were involved only in the combustion of propane to CO_2 and not in the formation of propene.

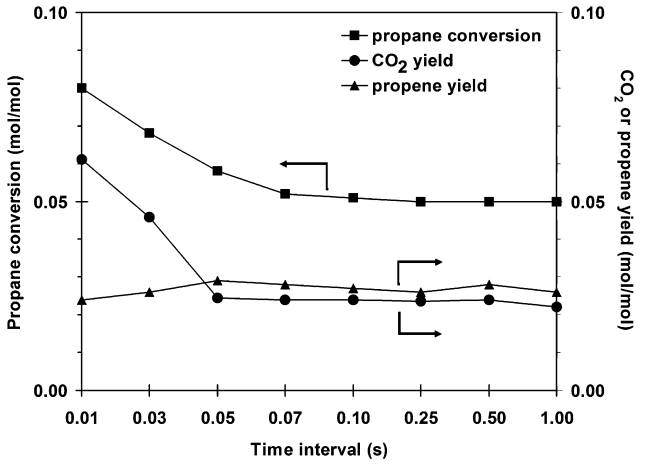

Fig. 10. Propane conversion and CO_2 or propene yield as a function of time interval at 773 K. (Alternating pulse experiment: O_2 pulsed first followed by propane, over Ti_HV330_H catalyst.)

6. General discussion

Supported vanadia catalysts were sputter-deposited either directly on the silica surface of nonporous bare beads or, through a sequential procedure, onto a preceding titania coating. In the latter double-deposition synthesis, a thick titania coating first ensured full coverage of the silica surface of the beads. From XRD and DRS, the sputter-deposited titania proved to be nanocrystalline anatase. According to some authors, this phase is preferred over rutile for enhancing the activity of the active vanadia layer [37], although others have found no true influence of the titania phase on vanadia activity [5,38]. In the discussion that follows, properties of the supported vanadia catalysts are compared as function of vanadia loading and the support type (either silica or anatase titania).

6.1. Vanadia dispersion

The dispersion of vanadia on both supports was evaluated by XPS and ICP data (Fig. 3). For the sputter-deposited catalysts, no difference in dispersion was found for vanadia on silica or on titania; a nearly linear relation between surface atomic ratios and bulk V loading indicates that for increasing sputter deposition time, the material was spread evenly over the surface.

From the literature, it is well accepted that titania has a positive effect on the dispersion of vanadia [39,40]. In contrast, on the silica surface of the bare beads, vanadia was expected to cluster or agglomerate into crystallites. Indeed, in many chemical preparation methods, silica is known to make vanadia agglomerate on its surface at relatively low coverage, due to the acid nature of both oxides [5]. This explains the accommodation of less surface vanadates in a monolayer on silica in comparison with other supporting oxides, such as TiO_2, Al_2O_3, ZrO_2, and Nb_2O_5 [6]. Nevertheless, several authors have reported that dispersion on silica can be steered by adjusting catalyst preparation conditions without altering the vanadia speciation [8,41]. Keränen et al. showed that the dispersion of vanadia up to monolayer coverage on silica or titania/silica could be improved by using ALD (atomic layer deposition) [42–44]. Inumaru et al. found that CVD-prepared vanadia/silica yielded better dispersion than impregnated catalysts [9].

The similar dispersion of vanadia on silica and titania in the present work suggests that the synthesis through magnetron sputtering has a positive influence on the dispersion over silica. On most support materials, sputter deposition initially yields island growth with homogeneously spread nuclei, the size of which is governed by the surface energies of the different materials [13]. For longer depositions, the nuclei grow and coalesce

to form a closed coating. In the sputtering process, additional energy is supplied to the nuclei or coating, from (unintentional) substrate heating and/or bombardment with energetic particles, which favours surface mobility and hence diffusion. As a result, the depositions evolve to a homogeneous coating once the monolayer threshold has well been passed, as was evidenced from the TEM images on Ti_HV330_H. In this respect, the only difference expected for magnetron sputter deposition of vanadia on silica or titania is in the initial nuclei size and shape, not their dispersion. For larger amounts of deposited vanadia, smooth coatings will form irrespective of the nature of the support. Hence, the observed similarity of vanadia dispersion on different supports can be considered an intrinsic result of the synthesis method.

6.2. Apparent surface density

The vanadia loading on the two support types was varied by adjusting the sputter deposition time from a very short 5 min up to 330 min. The deposited amounts of vanadia were very low for all catalysts (<0.01 wt%), far below the typical values of several wt% obtained for classically prepared catalysts. However, because the specific surface area of the support was equally low (0.0049 $m^2\,g^{-1}$), the apparent surface density, expressed as total amount of V per nm^2, was again comparable to the classical ones. All surface densities are reported in Table 2. Note that for the vanadia/titania catalysts, a 5% larger specific surface area was used, as the AFM image for the Ti_H support showed a slight increase in surface area (see Section 4.1.2). The surface densities for the vanadia/titania catalysts can be compared with the ones for two standard supported vanadia catalysts, the EUROCAT vanadia/titania EL10V1 and EL10V8 [7]. The latter were prepared by mixing powder TiO_2 with a vanadyl oxalate solution, followed by drying and calcination. EL10V1 is a catalyst with a vanadia monolayer loading onto titania, whereas EL10V8 was loaded with several vanadia layers, leading to the presence of some crystalline V_2O_5. For these catalysts, a surface density of 6.44 V nm^{-2} (resp. 51.86 V nm^{-2}) was determined.

6.3. Number of (mono)layers

From the apparent surface densities, a theoretical number of layers can be obtained for each vanadia loading in the assumption of homogeneous coverage. Several densities for "theoretical monolayer coverage" have been explored in the literature. A density of 10 V nm^{-2} follows from the V_2O_5-unit cell dimensions [6,45], which were already used to estimate the monolayer threshold (Sections 4.2.1 and 4.2.2). However, this density assumes a crystalline structure of the deposition, which is not necessarily the case, at least not for all loadings.

Compared with other oxide supports, silica is reported to accommodate only isolated monovanadates with a surface vanadia density ranging from 0.7 VO_x nm^{-2} to maximum 2–3 VO_x nm^{-2} [6,39]. However, there are indications that, depending on the preparation method, polyvanadates can form on a silica support [9]. Raman and EXAFS measurements on CVD-prepared vanadia/silica have shown the presence of V–O–V bonds in the vanadia layers, reflecting the formation of polyvanadates on silica [9].

For the sputter-deposited vanadia/silica catalysts, the dispersion was found to be quite similar on silica and titania supports. Thus, it is likely that the aforementioned low theoretical monolayer coverage on silica pertains only to the thinner depositions. Indeed, in direct contact with silica, the surface energy will fully influence the nucleation and growth mode of the first deposited vanadia. However, once a full monolayer of vanadia is deposited, the newly arriving material is no longer forced into this low-surface density framework and can grow in denser layers. This process is aided by the additional energy supplied by the magnetron sputter deposition process, which enhances surface mobility and diffusion.

To calculate the number of vanadia layers on silica, an average of 2.5 (±0.5) VO_x nm^{-2} was used as the theoretical monolayer coverage for the thinner depositions in samples $V5_H$ and $V15_H$. At this point, close to a theoretical monolayer of vanadia on silica was present. For the catalysts with longer deposition times, a theoretical density of 7.5 VO_x nm^{-2} was assumed above the first layer's 2.5 VO_x nm^{-2}, reflecting the accommodation of vanadia into more dense polyvanadate layers, once the first monolayer was completed. The resulting theoretical numbers of layers for the vanadia/silica catalysts are given in Table 2 (left part). The coverage ranged from below the theoretical monolayer to about 20 polyvanadate layers for the longest sputter deposition.

For the vanadia/titania catalysts, the theoretical polyvanadate monolayer coverage lies between 7 and 8 VO_x nm^{-2} [45,46]. Using an average value of 7.5 (±0.5) VO_x nm^{-2}, we end up with a coverage ranging from below 1 up to 16 theoretical polyvanadate monolayers for the titania-supported vanadia, with the monolayer border at 15 min deposition time, Ti_HV15_H (Table 2, right part).

6.4. V speciation and degree of polymerization

Absorption edge energies can be extracted from DRS [47]. The latter can be used to elucidate the local structure of V^{5+} and to determine the degree of polymerization of vanadia, because the position of the low-energy LMCT correlates with the domain size of vanadia [48], which increases with decreasing absorption edge energy. Indeed, electron transfer from the highest occupied molecular orbital (HOMO) of the ligand (here the lattice oxygen) to the lowest unoccupied molecular orbital (LUMO) in V^{5+} requires less energy, and thus occurs much easier, when V^{5+} is polymerized in large vanadia domains.

The absorption edge energies of the sputter-deposited catalysts were calculated using Tauc's law [49] and are given in Table 3. The energy was derived as the x intercept of a linearized near-edge region for $[F(R_\infty)h\nu]^{1/2}$ plotted against $h\nu$, where $F(R_\infty)$ is the Kubelka–Munk function and $h\nu$ is the energy of the incident light. Plotting the absorption edge energies for the sputter-deposited catalysts $Vtime_H$ and Ti_HVtime_H (Fig. 11) shows that they decreased with increasing apparent surface density, indicating increasing size of the vanadia do-

Table 3
Edge energies in eV as determined from the DRS spectra, number of covalent bonds (CVB number[a]) and molecular structure following [41,47] for all catalysts (m: minor, d: dominant).

Sample	Edge energy (eV)	CVB number	Molecular structure
Ti_HV5_H	3.63	0.00	Isolated VO_4
Ti_HV15_H	3.55	0.01	Isolated VO_4
Ti_HV30_H	3.09	1.82	Polymeric VO_4(d) + isolated VO_4(m)
Ti_HV60_H	2.8	2.97	Polymeric VO_4(d) + polymeric VO_6(m)
Ti_HV150_H	2.7	3.37	Polymeric VO_4(d) + polymeric VO_6(m)
Ti_HV330_H	2.64	3.60	Polymeric VO_4(m) + polymeric VO_6(d)
$V5_H$	3.39	0.64	Isolated/dimeric VO_4
$V15_H$	3.33	0.88	Dimeric/polymeric VO_4
$V30_H$	2.95	2.38	Polymeric VO_4
$V60_H$	2.85	2.77	Polymeric VO_4(d) + polymeric VO_6(m)
$V150_H$	2.71	3.33	Polymeric VO_4(d) + polymeric VO_6(m)
$V330_H$	2.6	3.76	Polymeric VO_4(m) + polymeric VO_6(d)

[a] CVB number determined following the formula in [47]: CVB = $14.03 - 3.95E_g$ (±0.34).

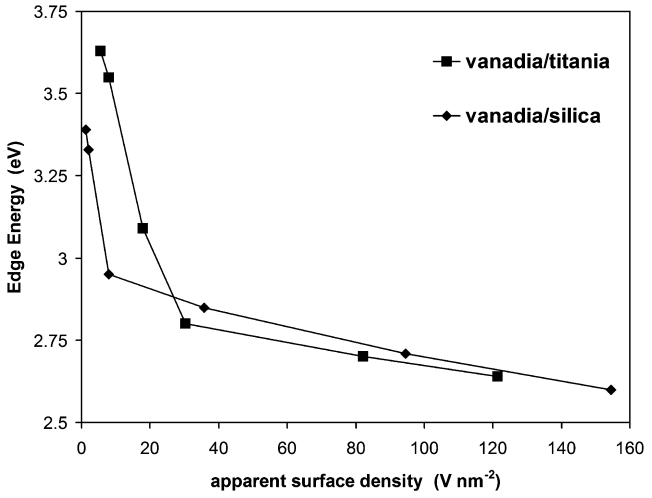

Fig. 11. Dependence of the UV–vis absorption edge energy on the apparent vanadia surface density for catalysts Ti_HVtime_H and $Vtime_H$.

mains. These results are consistent with trends reported earlier for various supported metal oxide catalysts [21,48,50].

The absolute values of edge energy obtained for the sputter-deposited catalysts and their corresponding degree of polymerisation can be evaluated by comparing them with the edge energies for vanadia reference compounds as reported by, for instance, by Gao et al. [41]. The resulting assignments are given in Table 3. In addition, the degree of polymerisation can be quantified using an empirical formula relating edge energy to the number of covalent bonds V–O–V (CVB number), as introduced by Weber for Mo oxides [48] and improved for use with supported vanadium oxides by Gao and Wachs [47]. Following this formula, the CVB number for bulk V_2O_5 amounts to 4.86, reflecting the number of second neighbours in the crystalline lattice. The resulting numbers are also reported in Table 3.

For the vanadia/titania catalysts Ti_HVtime_H, the edge energy was around 3.6 eV for the shortest deposition times, 5 and 15 min, which is characteristic of VO_4 either in dimeric or isolated form (Table 3). The zero value for the CVB number supports this assignment. Gao et al. found that for bilayered $V_2O_5/TiO_2/SiO_2$, loadings of 1, 5, and 10 wt% V_2O_5 (i.e., up to monolayer coverage) on different TiO_2 loadings yielded edge energies in the range of 3.4–3.8 eV [51]. Hence, the present high edge energy values of Ti_HV5_H and Ti_HV15_H were consistent with their (sub-) monolayer vanadia coatings.

For 30 min sputter time, the edge energy decreased to about 3 eV, which, from comparison with the vanadia reference compounds, relates to polymerized VO_4. From sputter deposition times of 60 min and up, the edge energy dropped to 2.8–2.6 eV, values typical for polymerized VO_6 [41]. Indeed, bulk V_2O_5 consisting of completely 3D polymerized VO_5/VO_6 exhibits the lowest edge energy value of 2.3 eV [52,53].

The foregoing assignment follows the evolution of bands observed in the DRS spectra, where the low energy absorbance increased at the expense of the higher energy absorbance, with increasing V loading (Fig. 6). For the intermediate samples, a mixed molecular structure was present. In between the two absorbance regions, an isobestic point with equal contribution of both coordinations appeared at around 29,000 cm^{-1}.

Edge energy values for the vanadia/silica catalysts showed a similar evolution with V surface density. Gao et al. reported edge energies of 3.4–3.6 eV for dehydrated V_2O_5/SiO_2 with 1–10% loading [41,47,51]. These values were attributed to isolated VO_4. For higher loadings of 12% and 15% V_2O_5/SiO_2, a slightly lower value of 3.34 eV (resp. 3.3 eV) was reported and ascribed to the presence of isolated VO_4 accompanied by some V_2O_5 crystallites [41,51]. The surface densities in their work remained low compared with ours (maximum 3.3 V nm^{-2} for 15% V_2O_5/SiO_2). Similarly, Tian reported a nearly constant edge energy of 3.5 eV for 1–12% V_2O_5/SiO_2, which was ascribed to monomeric VO_x [54]. Therefore, the edge energies found here for $V5_H$ and $V15_H$ agree with those for dehydrated V_2O_5/SiO_2, corresponding to predominantly isolated VO_4.

For higher loadings of vanadia on silica, it is thought that next to the isolated VO_4 species crystalline V_2O_5 will form and that polyvanadates cannot be accommodated by the silica support [5]. However, as mentioned in Section 6.3, Inumaru et al. prepared highly dispersed vanadia on silica, present as thin overlayers, for loadings up to 16.9 wt% V_2O_5 and containing V–O–V polyvanadates [9]. Further, in a catalyst series of vanadia on mesocellular silica foams, different vanadia species, including monomers, polymers, and crystal species, were identified [55]. The corresponding edge energies showed a continuous variation from 3.3 to 2.3 eV with increasing V loading on the silica support, reflecting the transition from isolated VO_4 over polymerised VO_4 to the start of V_2O_5 crystallisation. Hence, given the specific synthesis method and the observed evolution of edge energy for the sputter-deposited vanadia/silica with increasing surface density, we follow the same molecular assignment used for Ti_HVtime_H and identify the vanadia species of $V30_H$, $V60_H$, etc., as increasingly polymerised vanadia, rather than as isolated VO_4 species plus crystalline V_2O_5.

Comparing the titania and silica supports showed that the edge energies indeed did not differ much, indicating similar

degrees of polymerisation. Differences were seen only for the lowest surface densities/deposition times. From the corresponding CVB numbers, we can conclude that for both Ti_HV5_H and Ti_HV15_H, truly isolated VO_4 were present (CVB = 0), whereas on their corresponding silica supported counterparts, $V5_H$ and $V15_H$, the VO_4 was slightly dimeric or oligomerized (CVB = 0.6–0.9). This is consistent with recent findings of Tian et al., who quantified the amount of monomeric to polymeric vanadia in coatings with sub-monolayer coverage (edge energies of 3–3.6 eV). These authors determined a linear relationship between edge energy and the fraction of monomeric vanadia species from a series of physical mixtures of purely monomeric and polymeric VO_4 [54]. Applying this relation to the sputter-deposited catalysts, Ti_HV5_H and Ti_HV15_H contained a 100% monomeric VO_4, whereas $V5_H$ and $V15_H$ consisted of 70% (resp. 60%) monomeric vanadia and the remainder polymeric vanadia. For the higher surface densities, at 30–330 min of sputter time, polymerization increased and a mix of polymerized VO_4 and VO_6 was present. The difference in edge energy and CVB number between the two supports has faded, pointing to an equal degree of polymerisation. This agrees with the finding that for larger V loadings, octahedral vanadia began to dominate and vanadia was increasingly deposited onto vanadia, so that the support influence was gradually suppressed.

6.5. Reducibility

The support TiO_2 has been reported to be nonreducible in H_2-TPR up to 1230 K [6,56]. In contrast, Arena et al. found evidence for a reduction peak on a TiO_2 P25 support, with T_{max} lying at 850 K [57]. In another paper, the TPR profile of TiO_2 anatase powder consisted of a broad reduction feature ranging from 823 to 1047 K [58]. The EUROCAT TiO_2 support EL10 also displayed a small TPR peak, situated around $T_{max} \sim 822$ K on average [7]. Hence, in the present work's temperature range, the TPR measurements on $Ti_HV\mathit{time}_H$ might contain a contribution of the underlying titania.

Many papers dealing with TPR on vanadia/titania have reported only a single reduction peak. For densities remaining below 7–8 V nm^{-2}, values below 800 K were usually found [40,56], assignable to monovanadate [59]. The latter work reported that polyvanadate gave rise to a reduction peak at around 800 K, and that T_{max} was around 850 K for amorphous V_2O_5 and at 950 K or higher for crystalline V_2O_5. The latter assignment for different species indicates that with increasing surface density, the reducibility decreased as T_{max} shifted to higher values. This trend was observed by several other authors for titania-supported catalysts with increasing V loading [59–61].

In contrast, Arena et al. observed several T_{max} in H_2-TPR measurements for a vanadia/titania catalyst with 8 V nm^{-2} surface density (i.e., close to monolayer coverage) [57]. These authors performed a fit of the TPR spectra that resulted in five distinct contributions: 697 and 745 K, assigned to isolated "surface" vanadate species; 798 K, due to bidimensional polymeric species; and 892 and 1010 K, originating from octahedral V species and crystalline V_2O_5. Nalbandian and Lemonidou [62] found different TPR peaks: at 799 and 835 K for sub-monolayer densities, along with an additional peak at 871 K for the above-monolayer surface density of 25.6 V nm^{-2}. For vanadia supported on anatase with 6 V nm^{-2}, three peaks were reported, at 668, 794, and 938 K [63]. On the Eurocat samples EL10V1 and EL10V8 [7], 1 peak and 2 peaks, respectively, were observed at 850 and 930 K [62]. These temperatures were 50–60 K higher than those reported for their own prepared samples, reflecting a lower reducibility, which was ascribed to the presence of P and K impurities in the pigment-grade Eurocat support. Table 4 summarizes the temperatures of H_2 reduction peaks for different vanadia species reported in the literature. The results for the Eurocat samples are omitted due to impurity of the support.

Table 4
Summary of vanadia species and corresponding T_{max} literature values from H_2-TPR measurements (results from [57,59,62,63])

V species	Reported T_{max}
Monovanadate	668 K, 697 K, 745 K, <800 K
Polyvanadate	794 K, 798 K, 800 K, 835 K
Octahedral V/amorphous V_2O_5	850 K, 892 K
Crystalline V_2O_5	938 K, 950 K, 1010 K

With these literature data in mind, a tentative assignment can be made for the peaks in the TPR spectra of Fig. 7. In general, the onset and major reduction temperature for the sputter-deposited catalysts are found to increase with increasing surface density, in agreement with the literature [51,59–61]. For the lower surface density (Ti_HV15_H), mainly surface vanadate species in monomeric and dimeric form are present (620 and 715–720 K). The peak at 870 K could have originated from amorphous V_2O_5, but most likely is linked to reduction of the titania layer [57], because it was present only in the spectrum of Ti_HV15_H with the lowest surface density. The TPR spectrum for Ti_HV60_H showed an increased intensity of the peak at 715–720 K. Based on the literature assignment in Table 4, this temperature should equally correspond to "surface" vanadia species. However, because this catalyst's surface density was significantly higher and its edge energy decreased (Table 3), polymerisation of the vanadia must have occurred. From this point of view, T_{max} at 715–720 K should represent polymeric rather than dimeric or isolated species. This peak possibly should be considered a merged peak with several vanadia contributions (isolated + polymerized). In Ti_HV330_H, finally, strongly polymerized species dominated (with a peak at 790 K), still accompanied by surface species (705 and 660 K). In addition, the feature at 950 K can be attributed to the start of crystallisation of vanadia into V_2O_5 and can be assigned to the reduction of bulk V_2O_5 to V_6O_{13} [21]. Such a co-appearance of species on Ti_HV330_H agrees with observations of Argyle et al., who found from Raman measurements on VO_x/alumina that for surface densities above the monolayer, V_2O_5 crystallites were accompanied by monovanadates [64].

The TAP multiple-pulse reduction experiments with propane over $Ti_HV\mathit{time}_H$ yielded complete reduction of Ti_HV5_H to Ti_HV60_H, indicating that in these catalysts, all V is accessible for propane reduction [35]. On the other hand, catalysts Ti_HV150_H and Ti_HV330_H were less reducible. Because these catalysts consist of highly polymerized and crystalline vana-

dia, their lower degree of reduction reflects lower reducibility of their vanadia species and/or lower accessibility due to the presence of vanadia multilayers.

6.6. Activity

The ODH of alkanes over reducible oxides generally follows a Mars–van Krevelen (MvK) mechanism [65,66]. According to this mechanism, the alkane molecule reacts with lattice oxygen to produce an alkene and/or carbon oxides. Gas-phase oxygen replenishes the lattice oxygen through reoxidation of the reduced catalyst. As in TAP experiments, the propane ODH reaction occurs over the catalyst beads in absence of gas-phase oxygen, the MvK mechanism is indeed valid. The alternating-pulse experiment (Section 5.3.2) further showed that in the ODH reaction mostly lattice oxygen was consumed, whereas weakly adsorbed oxygen from the gas phase was responsible for the direct combustion of propane.

In TAP experiments, the silica support showed no activity for the ODH of propane. For the titania support, Ti_H, 3% propane conversion was found from quantitative analysis of reduction and reoxidation single-pulse experiments, as well as an oxygen conversion of 18% on reduced Ti_H. The observed activity is in good agreement with the literature, in which the TiO_2 support reportedly shows a small oxygen uptake after H_2 reduction at 641 K [67]. Gao et al. observed some reduction/activity of pure TiO_2 and silica-supported TiO_2 in both H_2-TPR and methanol oxidation [51].

The activity of the vanadia/titania catalysts for the ODH of propane is dependent on sputter time; TAP conversion at 773 K and steady-state surface TOF at 823 K were at a maximum at 60 min of vanadia sputter time. Catalysts Ti_HV5_H–Ti_HV30_H, with loadings up to two monolayers, showed similar activity in TAP, indicating that all of their vanadia species are equally active and/or accessible. Surface TOF for Ti_HV5_H and Ti_HV15_H of deposition time yielded equal values, in agreement with the TAP transient measurements. Catalysts Ti_HV30_H and especially Ti_HV60_H exhibited slightly higher TOF, after which the specific activity dropped considerably for deposition times of 150 and 330 min (see Fig. 8).

In view of the TAP and TPR reducibility measurements, high activity on the sputter-deposited catalysts Ti_HV5_H–Ti_HV60_H correlates with the more reducible species (see Section 6.5). The same catalysts were fully reduced in a propane TAP multiple-pulse experiment [35].

Nonetheless, incomplete agreement exists between the observed T_{max} from H_2-TPR and the highest TOF. Based on the TPR spectra, the highest TOF would be expected for the shortest deposition times, because here the most reducible species (i.e., those with the lowest T_{onset}) were present. For the catalyst with the highest TOF (Ti_HV60_H), the main T_{max} shifted to somewhat higher values, implying lower reducibility. This apparent contradiction could be countered by the (unknown) relative amounts of V species present, resulting in the highest TOF over Ti_HV60_H due to the larger number of active sites and/or highest activity of the sites. On the other hand, Chen et al. reported that propane ODH and H_2 reduction reactions can be linked only to a certain extent, because they have other structural and chemical requirements [68]. As a result, supported vanadia can react differently to both reactions.

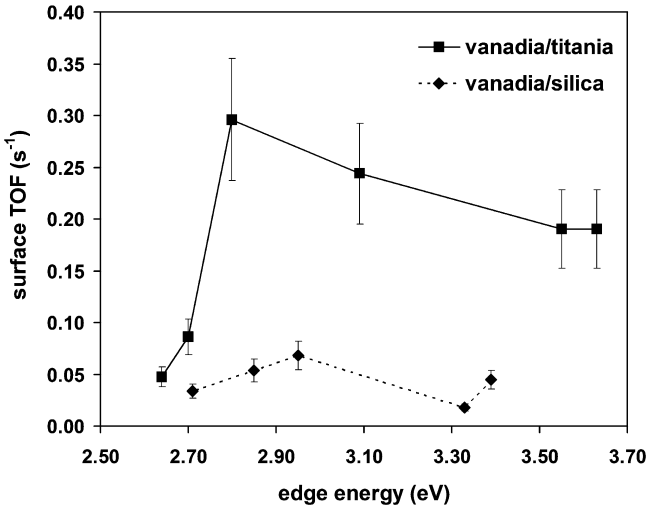

Fig. 12. Turnover frequencies versus edge energy for sputter deposited catalysts $Ti_HV\mathit{time}_H$ and singly coated samples $V15_H$, $V30_H$, $V60_H$, $V150_H$, and $V330_H$ (823 K; 20 vol% propane at 20 ml min^{-1}, 10 vol% O_2 balanced with helium); only the outer surface V atoms are taken into account.

For Ti_HV150_H and Ti_HV330_H, TAP conversion decreased in accordance with the previously reported lower degree of reduction in multiple-pulse experiments [35], demonstrating that a number of the vanadia sites are inaccessible and/or less active. Similarly, the activity per "surface" V [i.e., the surface TOF (Fig. 8)] displays decreased activity for Ti_HV150_H and Ti_HV330_H, which can then be ascribed only to the presence of less active vanadia species at the outer surface.

To directly relate the activity with the surface structure of the sputter-deposited vanadia/titania, we plotted the TOF data versus the corresponding edge energy (Fig. 12). Keeping in mind the correlation between edge energy and VO_x domain size and speciation (see Section 6.4), this figure can be interpreted as indicating that TOFs are low for the lowest edge energies (2.6–2.7 eV) which correspond to larger domains and bulk-like vanadia. Hence, the 3D polymeric V species that dominate these larger domains give rise to less reaction of the propane molecules, in agreement with the fact that multilayer vanadia is generally accepted to be less active [46,69]. For medium edge energies (2.8–3.2 eV), corresponding to smaller domains, the TOF per surface V has remarkably increased, even taking into consideration the error range. On the high edge energy end of the graph (3.5–3.7 eV), isolated vanadia still give rise to high surface TOF, albeit lower than for the medium-size domains.

In literature, it was reported that for ODH of propane at 606 K over vanadia/silica and vanadia/titania, the TOF per V increased with decreasing edge energy, thus increasing surface density, for densities up to polyvanadate monolayer coverage (7.5 V nm^{-2}) [70]. It was concluded that polyvanadates on titania were more active than isolated monovanadates. Then again, Wachs found constant TOF for surface densities up to monolayer vanadia/titania and concluded that isolated and polymeric vanadia species are equally active in propane ODH at

573 K [38]. Yet another paper reported decreased TOF with increasing density, related to the reduced number of V–O–support bonds per V atom on increasing polymerisation [69]. However, in the latter work reaction rates were normalised to the total number of V present, even for densities above the monolayer, implying that the authors considered all V equally active and accessible. The observed decrease of TOF with surface density above the monolayer could well be translated into a different trend when taking into account only the outer V as active species. Hence, the literature reports no clear relationship between TOF for propane ODH and vanadia loading, and factors other than the surface density can influence the observations [6,69,71].

As in the present work on sputter-deposited vanadial/titania highest TOF was found for medium edge energies of 2.8–3.2 eV, polymerised tetrahedral vanadia was more active than isolated species (see Table 3). This could relate to the need to have two V atoms available for activation of a propane molecule [68,72], in which case the polymeric tetrahedral vanadia, presenting a larger apparent surface density, would entail higher activity.

It is important to note here the high TOF values over the sputter-deposited catalysts Ti_HV5_H–Ti_HV60_H. For the ODH of propane at 823 K, a rate of formation of the order of ∼0.2–0.3 molecule of propene per (surface) V per second was obtained; this is significantly higher than that reported over classically prepared systems, which are generally in the range of 0.001–0.1 s^{-1} [46,71,73–76].

For the sputter-deposited vanadia/silica catalysts, the surface TOF showed less variation with V loading. Moreover, TOF always remained considerably lower than for the corresponding vanadia/titania catalysts. Similar observations for silica supports have been reported and ascribed to the presence of inactive isolated vanadia and active but poorly dispersed V_2O_5 [70].

For the shortest deposition times (5 and 15 min), a significant difference in activity with respect to the vanadia/titania catalysts was noted. According to DRS findings, isolated monovanadates were present on both types of support, although slight differences in edge energy and CVB number point toward some dimerization on the silica support. For intermediate deposition times of 30 and 60 min, this difference in edge energy disappeared, but a considerable deviation in activity between vanadia supported on silica and on titania remained. Hence, the latter is determined not by the vanadia speciation, but rather by the support; the titania support enhanced the propane ODH activity compared with silica. Similar results in propane ODH have been reported previously [70]. For longer deposition times, the TOF evolved to similar values on both silica and titania, indicating suppression of the support influence at higher V loadings, where vanadia multilayers form (Table 2).

The maximum TOF was found for a sputter-deposited catalyst vanadia/titania Ti_HV60_H with an apparent surface density of 30 V nm^{-2}, yielding about four polyvanadate vanadia layers assuming a polyvanadate monolayer density of 7.5 V nm^{-2} (Table 2). DRS revealed that these vanadia had an intermediate degree of polymerisation (2.8 eV), with polymeric VO_4 dominating the upcoming polymeric VO_6 (Table 3). TPR for this catalyst showed good reducibility with a major contribution of T_{max} at 715 K. However, as mentioned in Section 6.5, the TPR literature relates this temperature not to polymerised species, but rather to "surface" vanadia. Nevertheless, given the calculated apparent surface density and the DRS findings (edge energy and CVB number), the presence of isolated surface species alone was very unlikely. Rather, a mixture of species was present, including a large number of polymerised vanadia, presenting greater reducibility than classically prepared catalysts with comparable surface densities. The latter species are responsible for the high activity of these sputter-deposited catalysts in the ODH reaction of propane.

Compared to Ti_HV60_H, the vanadia/silica catalyst $V60_H$ had similar apparent surface density (35.8 V nm^{-2}) and number of layers (5.4 polyvanadate layers). Based on XPS-ICP and DRS (Sections 6.1 and 6.4), dispersion and vanadia speciation were similar on titania and silica, resulting in equal edge energies (2.85 vs 2.80 eV, respectively). All of these data indicate that these catalysts are very comparable and that the support does not influence either of these properties. Nevertheless, the specific activity for both (series of) catalysts differs significantly, showing that the specific activity is steered by the nature of the support, not by altering the vanadia dispersion or speciation, but rather by affecting the catalytic characteristics of the active layer.

Several authors have stressed the importance of the nature of the support on ODH activity and the crucial role of the V–O–support bond in determining the activity of the supported vanadia catalyst [6,54,69,70]. In a review paper on mixed metal oxides, Wachs pointed out that the V–O–support bond is the catalytically active site and that mainly the electronegativity of the support's cation determines the reactivity in many oxidation reactions by controlling the electron density on the V–O–support bond [38]. In another paper comparing several supported vanadia catalysts up to monolayer loading, Deo and Wachs deduced that, assuming constant activity per catalytic site, the strength of the V–O–support bond determines the number of active sites and hence the TOF in methanol oxidation [77]. However, most of the aforementioned papers deal with monolayer catalysts, where the vanadia loading does not exceed a surface density of 7.5 or 8 V nm^{-2}. Because the highest TOF in the oxidative dehydrogenation of propane at 823 K was found for Ti_HV60_H, a catalyst with 30 V nm^{-2} and hence several polyvanadate layers, the question arises whether or how the V–O–support bond can still affect the activity of the outer surface vanadia.

Two distinct options are possible. First, a possible intermixing of material of the subsequent sputter depositions or incomplete coverage of the titania can occur. However, this seems to be contradicted by the TPR profile of Ti_HV60_H; compared with that of Ti_HV15_H, the peak that was related to the reduction of titania has disappeared (Section 6.5). Second, the support may affect several vanadia layers. The latter option finds support in a review work of Centi [3], who reported the existence of a separate vanadia phase on titania for densities between one and four equivalent monolayers. High-resolution TEM measurements visualised this phase on anatase, rutile,

and TiO_2(B) [78], which was designated as amorphous vanadia, containing distorted octahedral V^{5+}, in contrast with the crystalline V_2O_5 phase that appeared only above four monolayers. The amorphous vanadia phase was also mentioned by Bond et al. [34,79] and Baiker et al. [80], who deduced its existence from Raman and/or TPR measurements. It was reported that its formation is promoted by the first deposited vanadia, which interact strongly with the anatase, forming a modified titania surface [78,81,82]. The latter then acts as anchorage interface for the next vanadia layers [83]. In several reactions, this disordered or amorphous vanadia was found to constitute the most active phase, even more active than the true vanadia monolayer. Centi found a significant increase in activity for oxidation of *o*-xylene by adding up to five vanadia layers over the modified anatase titania surface [3]. Baiker et al. found that three to four layers (∼2 nm thick) were most active in the selective catalytic reduction (SCR) of NO [80]. Sanati et al. observed optimal activity in oxidation of toluene to benzaldehyde over vanadia multilayers, 5 theoretical ML thick [78].

Although to the best of our knowledge, little or no data on propane ODH over multilayer vanadia on titania are available, it seems plausible to ascribe our finding of the highest TOF in this reaction over four polyvanadate vanadia layers to the presence of such a disordered vanadia phase. The reported structure of this phase matches the findings in this work: a mixed tetrahedral–octahedral V^{5+} species. The difference in activity between Ti_HV60_H and $V60_H$ then originates from the unique ability of TiO_2, particularly the anatase phase, to stabilize the first vanadia layer through strong interaction into a restructured vanadia–anatase surface, which is capable of modifying the next three to five vanadia layers into an amorphous but very active vanadia layer.

7. Conclusion

Magnetron sputtering inside a rotating drum allowed the synthesis of model catalysts of supported vanadia (vanadia/silica and vanadia/titania) by physical deposition. The cleanliness and high reproducibility of the method ensures that the catalyst properties are fundamental, that is, independent of contamination or uncontrolled preparation. Two series with varying vanadia loadings were prepared, ranging in thickness from well below the theoretical monolayer up to several multilayers, the latter comprising nanocrystallinity. No difference in dispersion between the silica and titania supports was observed. The vanadia species and degree of polymerisation were identified throughout the range of surface densities: from isolated surface vanadates over polymeric species to strongly polymerized and some crystalline V_2O_5 for the highest vanadia loadings. In contrast to many literature reports, no evidence was found for a different speciation or degree of polymerisation on the two supports. From the derived edge energies and the calculated number of neighbouring covalent bonds CVB, a slight difference in domain size was seen between the two supports at only the lower vanadia loadings. This points toward a certain degree of dimerization of vanadia on silica, whereas truly isolated monovanadates were found on titania. Thus, the titania and silica supports exhibited equal dispersion, speciation, and degree of polymerization as fundamental properties of supported vanadia. This result is ascribed to the use of sputter deposition as a physical method for precisely controlling the design of vanadia catalysts, enabling homogeneous coating of supports, irrespective of their nature.

Comparison of the two supports now allows, for the first time to the best of our knowledge, isolation of the effect of the support on catalyst performance from other effects, such as dispersion and the polymerisation grade of supported vanadia. The catalytic properties of both catalyst series were tested using the oxidative dehydrogenation of propane in TAP and steady-state experiments. Remarkably high TOFs were observed over sputter-deposited vanadia/titania catalysts with vanadia loadings between one and four theoretical monolayers. Here, vanadia/silica catalysts with similar V densities performed far worse, proving that the titania sublayer fundamentally favours vanadia activity. Because the titania does not alter the vanadia dispersion or speciation, it can affect activity only by influencing the structure of the first deposited vanadia layer. The fact that the highest TOF was recorded for a vanadia/titania catalyst with four polyvanadate layers indicates the extent of this influence. Hence, the titania support steers the activity of the supported vanadia indirectly by promoting the formation of subtly distorted but very active material in up to four layers. DRS and TPR analysis showed that the structure of this layer comprises a mixture of surface and mainly polymerised VO_4 vanadia.

Acknowledgments

The sputter deposition was performed in a vacuum chamber sponsored by the action “Equipment for Materials Investigation 1997–2000” from the Flemish government (IWT). The authors are grateful to R. Van Paemel (UGent) for assistance with the sputter chamber, U. Demeter (UGent) for the XPS measurements, L. Van Meirhaeghe for the AFM images, O. Janssens for the XRD and SEM work, and W. Vermandel for the TPR measurements. This work was performed in the framework of a Concerted Research Action (GOA) financed by Ghent University, and of the Belgian Programme on Interuniversity Poles of Attraction initiated by the Belgian State, Prime Minister’s Office, Science Policy Programming (IUAP-V/03). B.F.S. and P.A.J. also thank the IDECAT programme. The authors assume all scientific responsibility.

References

[1] B. GrzybowskaSwierkosz, Appl. Catal. A 157 (1997) 263.
[2] J.P. Dunn, H.G. Stenger Jr., I.E. Wachs, Catal. Today 51 (1999) 301.
[3] G. Centi, Appl. Catal. A 147 (1996) 267.
[4] H. Bosch, F. Janssen, Catal. Today 2 (1988), v (preface).
[5] T. Blasco, J.M. López Nieto, Appl. Catal. A 157 (1997) 117.
[6] I.E. Wachs, B.M. Weckhuysen, Appl. Catal. A 157 (1997) 67.
[7] G.C. Bond, J.C. Védrine, Catal. Today 20 (1994) 1.
[8] B.M. Weckhuysen, D.E. Keller, Catal. Today 78 (2003) 25.
[9] K. Inumaru, M. Misono, T. Okuhara, Appl. Catal. A 149 (1997) 133.
[10] D. Vernardou, M.E. Pemble, D.W. Sheel, Surf. Coat. Technol. 188–189 (2004) 250.

[11] A. Dittmar, H. Kosslick, J.-P. Müller, M.-M. Pohl, Surf. Coat. Technol. 182 (2004) 35.
[12] J. Libuda, J.-H. Freund, Surf. Sci. Rep. 57 (2005) 157.
[13] J.E. Greene, in: D.T.J. Hurle (Ed.), Handbook of Crystal Growth, vol. 1a, Elsevier, Amsterdam, 1993.
[14] P. Albers, K. Seibold, A.J. McEvoy, J. Kiwi, J. Phys. Chem. 93 (1989) 1510.
[15] G.M. Veith, A.R. Lupini, S.J. Pennycook, G.W. Ownby, N.J. Dudney, J. Catal. 231 (2005) 151.
[16] B. Wang, Z. Ji, F.T. Zimone, G.M. Janowski, J.M. Rigsbee, Surf. Coat. Technol. 91 (1997) 64.
[17] H. Poelman, K. Eufinger, D. Depla, D. Poelman, R. De Gryse, B.F. Sels, G.B. Marin, in: CONCORDE conference, January 2006, Thessaloniki, Greece; Appl. Catal. A (2006), submitted for publication.
[18] H. Poelman, D. Poelman, D. Depla, H. Tomaszewski, L. Fiermans, R. De Gryse, Surf. Sci. 482 (2001) 940.
[19] H. Poelman, H. Tomaszewski, D. Poelman, L. Fiermans, R. De Gryse, Surf. Interface Anal. 34 (2002) 724.
[20] K. Chen, A.T. Bell, E. Iglesia, J. Phys. Chem. B 104 (2000) 1292.
[21] I.E. Wachs, Y. Chen, J.-M. Jehng, L.E. Briand, T. Tanaka, Catal. Today 78 (2003) 13.
[22] S.O. Shekhtman, G.S. Yablonsky, J.T. Gleaves, R. Fushimi, Chem. Eng. Sci. 58 (2003) 4843.
[23] J.T. Gleaves, J.R. Ebner, T.C. Kuechler, Catal. Rev. Sci. Eng. 30 (1988) 49.
[24] H. Tomaszewski, H. Poelman, D. Depla, D. Poelman, R. De Gryse, L. Fiermans, M.-F. Reyniers, G. Heynderickx, G.B. Marin, Vacuum 68 (2003) 31.
[25] H.G. Bachmann, F.R. Ahmed, W.H. Barnes, Z. Kristallogr. 115 (1961) 110.
[26] N. Li, A. Wang, Z. Liu, X. Wang, M. Zheng, Y. Huang, T. Zhang, Appl. Catal. B 62 (2006) 292.
[27] S. Klein, B.M. Weckhuysen, J.A. Martens, W.F. Maier, P.A. Jacobs, J. Catal. 163 (1996) 489.
[28] M. Schraml-Marth, A. Wokaun, A. Baiker, J. Catal. 124 (1990) 86.
[29] F. Arena, F. Frusteri, G. Martra, S. Coluccia, A. Parmaliana, J. Chem. Soc. Faraday Trans. 93 (1997) 3849.
[30] G. Centi, S. Perathoner, F. Trifiro, A. Aboukais, C.F. Aisi, M. Guelton, J. Phys. Chem. 96 (1992) 2617.
[31] U. Scharf, M. Schraml-Marth, A. Wokaun, A. Baiker, J. Chem. Soc. Faraday Trans. 87 (1991) 3299.
[32] H. Berndt, A. Martin, A. Brückner, E. Schreier, D. Müller, H. Kosslick, G.U. Wolf, B. Lücke, J. Catal. 202 (2001) 384.
[33] B.M. Weckhuysen, I.P. Vannijvel, R.A. Schoonheydt, Zeolites 15 (1995) 482.
[34] G.C. Bond, S.F. Tahir, Appl. Catal. 71 (1991) 1.
[35] I. Sack, V. Balcaen, M. Olea, H. Poelman, G.B. Marin, Catal. Today 112 (2006) 68.
[36] G.S. Yablonsky, M. Olea, G.B. Marin, J. Catal. 216 (2003) 120.
[37] A. Satsuma, S. Takenaka, T. Tanaka, S. Nojima, Y. Kera, H. Miyata, Appl. Catal. 232 (2002) 93.
[38] I.E. Wachs, Catal. Today 100 (2005) 79.
[39] I.E. Wachs, Catal. Today 27 (1996) 437.
[40] E. Heracleus, M. Machli, A.A. Lemonidou, I.A. Vasalos, J. Mol. Catal. A 232 (2005) 29.
[41] X.T. Gao, S.R. Bare, B.M. Weckhuysen, I.E. Wachs, J. Phys. Chem. B 102 (1998) 10842.
[42] J. Keränen, C. Guimon, E. Iiskola, A. Auroux, L. Niinistö, J. Phys. Chem. B 107 (2003) 10773.
[43] J. Keränen, P. Carniti, A. Gervasini, E. Iiskola, A. Auroux, L. Niinistö, Catal. Today 91–92 (2004) 67.
[44] A. Gervasini, P. Carniti, J. Keränen, L. Niinistö, A. Auroux, Catal. Today 96 (2004) 187.
[45] J. Haber, A. Kozlowska, R. Kozłowski, J. Catal. 102 (1986) 52.
[46] A. Khodakov, J. Yang, S. Su, E. Iglesia, A. Bell, J. Catal. 177 (1998) 343.
[47] X.T. Gao, I.E. Wachs, J. Phys. Chem. B 104 (2000) 1261.
[48] J. Weber, J. Catal. 151 (1995) 470.
[49] J. Tauc, R. Grigorovici, A. Vancu, Phys. Status Solidi 15 (1966) 627.
[50] K. Chen, S. Xie, A.T. Bell, E. Iglesia, J. Catal. 198 (2001) 232.
[51] X.T. Gao, S.R. Bare, J.L.G. Fierro, I.E. Wachs, J. Phys. Chem. B 103 (1999) 618.
[52] D.C. Conlon, W.P. Doyle, J. Chem. Phys. 35 (1961) 752.
[53] N. Kenny, C.R. Kannewurf, D.H. Whitmore, J. Phys. Chem. Sol. 27 (1966) 1237.
[54] H. Tian, E.I. Ross, I.E. Wachs, J. Phys. Chem. B 110 (2006) 9593.
[55] Y.-M. Liu, W.-L. Feng, T.-C. Li, H.-Y. He, W.-L. Dai, W. Huang, Y. Cao, K.-N. Fan, J. Catal. 239 (2006) 125.
[56] R.P. Singh, M.A. Banares, G. Deo, J. Catal. 233 (2005) 388.
[57] F. Arena, F. Frusteri, A. Parmaliana, Appl. Catal. A 176 (1999) 189.
[58] M.K. Maity, M.S. Rana, S.K. Bej, J. Ancheyta-Juárez, G. Murali Dhar, T.S.R. Prasada Rao, Appl. Catal. A 205 (2001) 215.
[59] D.A. Bulushev, L. Kiwi-Minsker, F. Rainone, A. Renken, J. Catal. 205 (2002) 115.
[60] M.A. Bañares, M.V. Martínez-Huerta, X.T. Gao, J.L.G. Fierro, I.E. Wachs, Catal. Today 61 (2000) 295.
[61] H.K. Matralis, Ch. Papadopoulou, Ch. Kordulis, A.A. Elguezabal, V. Cortes Corberan, Appl. Catal. A 126 (1995) 365.
[62] L. Nalbandian, A.A. Lemonidou, Thermochim. Acta 419 (2004) 149.
[63] S. Martinez, R. Morales, M.G. Cárdenas-Galindo, A.G. Rodríguez, F. Pedraza, B.E. Handy, Thermochim. Acta 434 (2005) 74.
[64] M.D. Argyle, K. Chen, A.T. Bell, E. Iglesia, J. Catal. 208 (2002) 139.
[65] P. Mars, D.W. Van Krevelen, Chem. Eng. Sci. 3 (1951) 41.
[66] K. Scheurell, E. Hoppe, K.-W. Brzezinka, E. Kemnitz, J. Mater. Chem. 14 (2004) 2560.
[67] G.T. Went, S.T. Oyama, A.T. Bell, J. Phys. Chem. 94 (1990) 4240.
[68] K. Chen, A.T. Bell, E. Iglesia, J. Catal. 209 (2002) 35.
[69] A. Christodoulakis, M. Machli, A.A. Lemonidou, S. Boghosian, J. Catal. 222 (2004) 293.
[70] A. Khodakov, B. Olthof, A.T. Bell, E. Iglesia, J. Catal. 181 (1999) 205.
[71] X.T. Gao, J.-M. Jehng, I.E. Wachs, J. Catal. 209 (2002) 43.
[72] F. Gilardony, A.T. Bell, A. Chakraborty, P. Boulet, J. Phys. Chem. B 104 (2000) 12250.
[73] R. Monaci, E. Rombi, V. Solinas, A. Sorrentine, E. Santacessaria, G. Colon, Appl. Catal. A 214 (2001) 203.
[74] G.G. Cortez, M.A. Bañares, J. Catal. 209 (2002) 197.
[75] T. Davies, S.H. Taylor, J. Mol. Catal. A 220 (2004) 77.
[76] J.M. López Nieto, J. Soler, P. Concepción, J. Herguido, M. Menéndez, J. Santamaría, J. Catal. 185 (1999) 324.
[77] G. Deo, I.E. Wachs, J. Catal. 146 (1994) 323.
[78] M. Sanati, L.R. Wallenberg, A. Andersson, S. Jansen, Y. Tu, J. Catal. 132 (1991) 128.
[79] G.C. Bond, J.P. Zurita, S. Flamerz, P.J. Gellings, H. Bosch, J.G. Van Ommen, B.J. Kip, Appl. Catal. 22 (1986) 361.
[80] A. Baiker, P. Dollenmeier, M. Glinski, A. Reller, Appl. Catal. 35 (1987) 351.
[81] G. Centi, E. Giamello, D. Pinelli, F. Trifiro, J. Catal. 130 (1991) 220.
[82] G. Centi, D. Pinelli, F. Trifiro, D. Ghoussoub, M. Guelton, L. Gengembre, J. Catal. 130 (1991) 238.
[83] G. Centi, D. Pinelli, F. Trifiro, J. Mol. Catal. 59 (1990) 221.